Published in final edited form as:
J Phys Chem B. 2008 July 17; 112(28): 8250–8256.

Structure and Thermotropic phase Behavior of Fluorinated Phospholipid Bilayers: A combined Attenuated Total Reflection FTIR Spectroscopy and Imaging Ellipsometry Study

Steffen Schuy[†], **Simon Faiss**[†], **Nicholas C. Yoder**[‡], **Venkateshwarlu Kalsani**[‡], **Krishna Kumar**[*,‡], **Andreas Janshoff**[*,†], and **Reiner Vogel**[*,§]

† *Institute for Physical Chemistry, University of Mainz, 55128 Mainz, Germany*

‡ *Department of Chemistry, Tufts University, Medford, Massachusetts 02155*

§ *Institute for Molecular Medicine and Cell Research, University of Freiburg, 79104 Freiburg, Germany*

Abstract

Lipid bilayers consisting of lipids with terminally perfluoroalkylated chains have remarkable properties. They exhibit increased stability and phase-separated nanoscale patterns in mixtures with nonfluorinated lipids. In order to understand the bilayer properties that are responsible for this behavior, we have analyzed the structure of solid-supported bilayers composed of 1,2-dipalmitoyl-*sn*-glycero-3-phosphocholine (DPPC) and of a DPPC analogue with 6 terminal perfluorinated methylene units (F6-DPPC). Polarized attenuated total reflection Fourier-transform infrared spectroscopy indicates that for F6-DPPC, the tilt of the lipid acyl chains to the bilayer normal is increased to 39° as compared to 21° for native DPPC, for both lipids in the gel phase. This substantial increase of the tilt angle is responsible for a decrease of the bilayer thickness from 5.4 nm for DPPC to 4.5 nm for F6-DPPC, as revealed by temperature-controlled imaging ellipsometry on microstructured lipid bilayers and solution atomic force microscopy. During the main phase transition from the gel to the fluid phase, both the relative bilayer thickness change and the relative area change are substantially smaller for F6-DPPC than for DPPC. In light of these structural and thermotropic data, we propose a model in which the higher acyl-chain tilt angle in F6-DPPC is the result of a conformational rearrangement to minimize unfavorable fluorocarbon–hydrocarbon interactions in the center of the bilayer due to chain staggering.

Introduction

Bilayers made of terminally perfluoroalkylated phosphatidylcholines (PCs) show remarkable differences in their structural and physical properties compared with bilayers composed of their pure hydrocarbon analogues. Santaella and co-workers have synthesized a series of F-alkyl modified phosphatidylcholines, that formed highly stable liposomes and are promising in biomedical applications.[1,2] Subsequent studies revealed several interesting properties of the perfluoroalkylated phospholipids, such as polymorphic phase behavior,[3] reduced membrane permeability,[4,5] rigidifying effect of the fluorinated bilayer core,[6] and high detergent resistance.[7] Models describing molecular packing of highly fluorinated phospholipid monolayers were proposed by Rolland et al., who observed an increase in the area per molecule upon partial substitution of hydrocarbon-chain segments with fluorocarbons.[8] McIntosh et al. have reported structural data on highly fluorinated phospholipid bilayers by using X-ray

* Corresponding authors. E-mail: reiner.vogel@biophysik.uni-freiburg.de, janshoff@uni-mainz.de, and krishna.kumar@tufts.edu.

diffraction and described different physical properties as compared to conventional bilayers.[9] On the basis of their data on the bilayer thickness of the fluorinated analogues, they further proposed a considerably increased chain tilt angle of the lipids to the bilayer normal. Although there is a lack of experimental data on the chain arrangement in fluorinated bilayers, a large number of researchers have analyzed the structure of self-assembled monolayers (SAMs) containing partially fluorinated alkyl chains,[10–16] from which insights into the physical driving forces for the distinct packing in fluorinated lipid bilayers can be derived. In all cases, fluorination of chain segments alters the tilt angle as compared to the pure hydrocarbon analogues; yet, both direction and degree of the change also depended strongly on the alkyl spacer length, the headgroup of the molecule, and the metal on which the SAM is deposited.[10–16]

This work focuses on determining tilt angles of both the hydrocarbon and the fluorocarbon segments in bilayers of 1,2-dipalmitoyl-*sn*-glycero-3-phosphocholine (DPPC) and of a partially fluorinated analogue of DPPC with 6 terminal perfluorinated methylene units (F6-DPPC), Figure 1A, by using polarized attenuated total reflection Fourier-transform infrared (ATR-FTIR) spectroscopy and relating these results to data obtained for the bilayer thickness, by using imaging ellipsometry and in situ atomic force microscopy (AFM). The results complement the findings of a recent study, in which a distinctive nanoscale domain patterning was found in supported lipid bilayers consisting of mixtures of hydrocarbon and fluorocarbon phospholipids, by using AFM.[17] This domain patterning consisted of regularly spaced stripes and constitutes a promising tool for the clustered display of ligands on surfaces of vesicles and on live cells.[18–21] In addition, several other phenomena were observed that required further investigation, such as a conspicuous height difference of 1.1 nm between fluorinated and unfluorinated lipid domains, although both lipids were apparently in the gel phase. Furthermore, a puzzling thermotropic behavior was observed, in which the absence of defects in a heating and cooling cycle posed questions concerning the change in lipid area during the main phase transition.[22–26] These questions are now tackled by scrutiny of the bilayer thickness and the relative area change $\Delta A/A$ during the main phase transition by using temperature-controlled imaging ellipsometry on microstructured bilayers.

Materials and Methods

Vesicle Preparation

Lipids were dissolved in chloroform and transferred into a test tube. After evaporation of the solvent in a stream of nitrogen at 55 °C for DPPC and 40 °C for F6-DPPC (all temperatures are well above the main phase-transition temperatures), the resulting lipid film was dried for 3 h in a vacuum oven at 55 °C. Large multilamellar vesicles (MLV) of DPPC were formed from 1 mg lipid film by hydrating the film in deionized water for 20 min at 60 °C and thorough vortexing. For the formation of MLVs from F6-DPPC, an extended hydration time of at least 45 min at 65 °C was necessary to obtain homogeneous suspensions. This step was repeated once with a reduced hydration time of 15 min, resulting in a homogeneous, turbid suspension. Small unilamellar vesicles (SUVs) were formed from MLVs of DPPC and F6-DPPC in standard buffer (10 mM Tris, 100 mM NaCl, pH 7.4) by sonification (50 W, 0.4 s pulse, 20 min) in a vessel resonator (Sonoplus HD 2070, Bandelin, Berlin, Germany), resulting in a clear opalescent suspension. The final lipid concentration (MLVs or SUVs) was 1 mg/mL in all experiments.

ATR-FTIR Experiments

ATR-FTIR experiments were performed by using a Bruker (Ettlingen, Germany) Vertex FTIR spectrometer. Spectra were acquired with an HgCdT detector at 2 cm^{-1} resolution with 1 min sampling time, by using Blackman–Harris 3-term apodization and a zero filling factor 2. IR-

band positions were determined from unpolarized spectra by curve fitting procedures by using the Bruker OPUS software.

Multilamellar films were produced by drying MLVs prepared from 1 mg of lipid in deionized water under reduced pressure on a 85 mm × 6 mm side of a trapezoidal germanium internal reflection element and were then mounted in a thermostatted custom-made ATR cell. Films were examined either in dry state or were hydrated from the vapor phase and equilibrated prior to the experiments.

For analysis of polarized spectra, we used the Harrick thick film or two-layer approximation[27] that was developed for films substantially thicker than the penetration depth of the evanescent field (~0.4 μm in our setup), which was the case in all experiments. Absorption spectra A_p and A_s were acquired with polarizations parallel (p) and perpendicular (s) to the plane of incidence by using a KRS-5 12000 grid polarizer (Graseby Specac, UK) on a rotatable mount. For visual inspection, these absorption spectra were converted into absorption spectra polarized in the *xy*-plane parallel to the surface of the ATR crystal and in the *z*-direction perpendicular to it, A_{xy} and A_z, respectively. This was achieved by decomposing the p- and s-polarizations into their *x*, *y*, and *z* electric field components with respect to the crystal surface in the Harrick thick-film formalism.[27–29] By using refractive indices $n = 4.01$ for germanium, $n = 1.48$ for DPPC,[30] and $n = 1.40$ for the fluorinated lipids,[14] the resulting equations for these conversions were $A_{xy} = A_s/j$, with $j = 2.310$ for DPPC and $j = 2.274$ for the fluorinated lipids, and $A_z = (A_p - kA_s)/l$, with $k = 0.845$ and $l = 2.667$ for DPPC and $k = 0.863$ and $l = 2.582$ for the fluorinated lipids.

The orientation of the transition dipole moment of a vibration was calculated directly from the dichroic ratio *R*.[27–29] *R* was determined by a previously developed formalism, which is relatively insensitive to baseline distortions.[31] The accuracy of the measured tilt angles was primarily limited by the achieved order parameter of the lipid films and is estimated to be approximately ±2°. All tilt angles are averages obtained from three independent measurements. Tilt angles were further used to extract the height differences by a simple model (Figure 6). The apparent lipid length of 2.8 nm was calculated by using the steric bilayer thickness d_B = 4.78 nm of hydrated DPPC bilayers and a chain tilt of 31°.[32,33]

Formation of Microstructured Lipid Bilayers

Structured solid-supported lipid bilayers were fabricated by micromolding in capillaries. Therefore, the poly dimethyl-siloxane (PDMS) mold was attached to a hydrophilic substrate (glass or silicon), forming a hydrodynamic network. Capillaries were filled with a suspension of SUVs in buffer to form a planar supported bilayer. After bilayer formation, the stamp was peeled off and the surface was extensively rinsed with buffer. Without drying, the substrate was mounted into the accordant fluid measurement cells. A detailed description on the formation of microstructured lipid bilayers on glass or silicon and imaging via temperature-controlled AFM and temperature-controlled imaging ellipsometry, as well as the geometric design of the PDMS mold, is given elsewhere.[34–38]

Ellipsometry

Ellipsometry is a non-invasive, well-established method for the characterization of ultra-thin films in terms of layer thickness and refractive indices.[39–42] In principle, the change of the state of the polarization of monochromatic parallel light upon reflection of a film-covered surface is measured. The resulting changes in the state of polarization can be expressed and quantified by the ellipsometric angles Δ and Ψ. These angles are related to the complex reflectance ratio ρ

$$\rho = R_P / R_S = (\tan\Psi)\, e^{i\Delta} \quad (1)$$

where R_P and R_S are the overall refractive coefficients parallel and perpendicular to the surface, respectively. The ellipsometry angles are sensitive to the interfacial architecture, and thus, they can be related to the layer thickness for homogeneous thin films by means of model calculations based on Fresnel equations. In this study, a commercially available imaging ellipsometer (EP^3-SW, Nanofilm Technologie, Göttingen, Germany) was used to determine the thickness d and the relative area change $\Delta A/A$ during the main phase transition of the structured lipid bilayers. Data acquisition and analysis followed previous protocols,[38] using refractive indices $n = 1.53$ for a fully hydrated DPPC bilayer[38] and $n = 1.40$ for F6-DPPC.[14] In brief, the average bilayer thickness was first measured by a four-zone nulling procedure in several sections or regions of interests by using the silica substrate as a reference, and the thickness calculations were accomplished by employing the respective layer model. For the determination of the thermal expansion of a bilayer $\Delta A/A$ during the main phase transition, microstructured bilayers consisting of DPPC or F6-DPPC were imaged at different temperatures by ellipsometry, resulting in a Δ-map, which displays the ellipsometric angle Δ over the whole image with approximately 1 μm resolution and from which the thickness for each pixel was computed. From the Δ-maps for each temperature, we determined the fractional area change $\Delta A/A$ by a histogram analysis of the image section. For illustration, the Δ-maps obtained from imaging ellipsometry of microstructured F6-DPPC and DPPC bilayers in the gel and in the fluid phase are given as insets in Figure 3 (see Supporting Information).

AFM

Experiments were carried out in aqueous solutions by using a commercial scanning force microscope (Dimension 3100 with Nanoscope IIIa+A/D controller, Veeco Digital Instruments, Santa Barbara, CAS) with silicon nitride cantilevers (OMCL-TR400PSA, Olympus, Japan), exhibiting nominal spring constants of 0.08 N/m. Imaging was performed in tapping mode at controlled temperature in aqueous solution. The ratio of the damped and free cantilever oscillation amplitude A_{sp}/A_0 during imaging was adjusted to 0.85. Images were postprocessed, and averaged height profiles were taken by using SPIP image processing software (Version 2.2002, Image Metrology, Lyngby, Denmark).

Results

Orientation of Fluorinated DPPC in Dry Multilamellar Bilayers

To determine the tilt angle of the hydrocarbon side chains in partially perfluorinated DPPC analogue (F6-DPPC) with respect to the bilayer normal, we used polarized ATR-FTIR spectroscopy on oriented multilamellar stacks of bilayers deposited on the surface of the ATR crystal. Polarized absorption spectra were measured with polarizations parallel and perpendicular with respect to the plane of incidence and were decomposed into absorption spectra polarized parallel and perpendicular to the crystal surface, A_{xy} and A_z, respectively, as detailed in the Materials and Methods section.

In Figure 1 B, absorption spectra polarized parallel A_{xy} and perpendicular A_z to the plane of the ATR crystal are shown in the range of the hydrocarbon and fluorocarbon stretching vibrations for dry F6-DPPC multilamellar films in the gel phase (L_C) at room temperature, revealing the dichroic nature of these absorption bands. The absorption band at 2852.5 cm^{-1} contains the symmetric CH_2 stretch of the hydrocarbon moiety, with the transition dipole moment of this vibration oriented perpendicular to the chain axis. By comparing absorption spectra of F6-DPPC with those of DPPC (Figure 1C), the fluorocarbon-associated bands in the range between 1100 and 1400 cm^{-1} could be distinguished. On the basis of previous studies on fluorinated fatty acids,[16] the F6-DPPC band at 1144 cm^{-1} was assigned to the symmetric

CF_2 stretch, whereas the bands at 1237 and 1191 cm^{-1} contain the antisymmetric CF_2 stretch. The bands at 1320 and 1367 cm^{-1} were assigned to the symmetric and antisymmetric CF_3 stretches, respectively. In contrast to the CF_2 stretch, the transition dipole moment of the CF_3 stretch is oriented in the direction of the final C–C bond and thus under an angle of only about 30° to the chain axis. It yields therefore a dichroism inverse to that of the CF_2 stretching vibrations as can be easily discerned in the right panel of Figure 1B.

By focusing on the symmetric stretch vibrations of the CH_2 groups at 2852.5 cm^{-1} and of the CF_2 groups at 1144 cm^{-1}, the orientation of the transition dipole moment of the vibration can be determined from their dichroic ratio with respect to the crystal surface. Assuming an orientation of the bilayer plane parallel to the crystal surface and of the transition dipole moment perpendicular to the molecular chain axis, apparent tilt angles of the chain axis with respect to the bilayer normal can be independently calculated for the hydrocarbon and the fluorocarbon moieties. Evaluation of the respective stretching bands of F6-DPPC yields an apparent tilt angle of 38° for the hydrocarbon chain and a slightly larger angle of 41° for the fluorocarbon chain. By averaging these values weighted by the approximate length of the respective chain moiety, a tilt of the F6-DPPC side chain of 39° is obtained in dry gel phase lipid. This value compares with a tilt of 21° for DPPC measured under the same conditions (inset in Figure 1B and Table 1). The derivation of the tilt angle from the dichroic ratio of the CH_2 stretch of F6-DPPC depends on the assumption that the hydrocarbon segment forms an ordered all-trans chain. The position of the methylene stretch at 2852.5 cm^{-1} in F6-DPPC is relatively high compared with 2850 cm^{-1} in DPPC. It cannot be excluded that this upshift reflects already some disordering in the hydrocarbon moiety of F6-DPPC, even at low temperature, in the dry film (see Discussion). In that case, the determined tilt angle listed in Table 1 would be strictly valid only for the rigid CF_2 moiety of F6-DPPC.

Thermotropic Phase Behavior of Supported Fluorinated DPPC Bilayers

The phase transition of fluorinated DPPC analogues was also followed by using ATR-FTIR spectroscopy, with the positions of the CH_2 stretching vibrations being sensitive indicators for the occurrence of *gauche* conformations during chain melting. At 15 °C, hydrated F6-DPPC films are in the gel phase, and the position of the symmetric CH_2 stretch is similar to that in dry films at the same temperature (Figure 2). As the temperature is raised past the T_M, an unusually large upshift of the peak by 4.8 cm^{-1} is observed, indicating the formation of melted hydrocarbon chain segments in the fluid phase (L_α). Interestingly, no significant shift is observed for the absorption peak of the symmetric stretch of the CF_2 moiety.

In further experiments, the impact of the phase transition on the apparent tilt angles of F6-DPPC was studied. In dry multilamellar films, an increase of the apparent tilt angle by approximately 5° was observed upon heating from 10 to 50 °C, accompanied by a shift of the absorption peak of the CH_2 stretching vibration similar as that in hydrated multilamellar films (data not shown). A similar analysis of the tilt angle in hydrated films is complicated by the decrease of the order parameter of the multilamellar films upon hydration, which reduces the reliability of such measurements.

In our previous study, the phase-transition temperature, T_M, for multilamellar F6-DPPC vesicles was determined by differential scanning calorimetry (DSC) to be 25 °C, and a substantially reduced melting enthalpy compared to pure DPPC was found,[17] corresponding reasonably well to the data reported by Santaella and co-workers for similar fluorinated lipids.[3]

In order to investigate further the gross structural changes which occur in the bilayer during phase transition, we employed two high resolution, variable-temperature techniques: imaging ellipsometry and AFM. Microstructured DPPC and F6-DPPC bilayers were imaged during a

heating cycle, starting at temperatures well below the phase transition temperature of the respective phospholipids (Figure 3). During the heating cycle, the temperature was varied from 15.2 to 37.9 °C for F6-DPPC and from 23.9 to 63.9 °C for neat DPPC bilayers. The ellipsometric data reveal a decrease of the bilayer thickness during the transition from the gel to the fluid phase from 5.4 nm (23.9 °C) to 3.4 nm (52.4 °C) in DPPC, whereas the thickness of F6-DPPC bilayers decreased only marginally from 4.5 nm (15.2 °C) to 3.9 nm (37.9 °C), Tables 1 and 2. The bilayer thicknesses obtained for DPPC in the gel and in the fluid phase are in good agreement with previously published results determined independently by AFM.[25, 43] Additional experiments employing temperature-controlled AFM on microstructured solid-supported F6-DPPC bilayers confirmed the membrane thickness data measured by ellipsometry (Figure 4). These experiments were conducted by microstructuring bilayers (as described in the Materials and Methods section) and measuring the layer thickness by averaged line scan over the edges of the bilayer. We obtained an average thickness of 4.5 nm for the L_C phase (12 °C) and 4.1 nm for the L_α phase (35 °C), in agreement with the ellipsometric data.

Imaging ellipsometry further revealed a very low relative area change $\Delta A/A$ during the phase transition of only 0.05 ± 0.01 for F6-DPPC bilayers, whereas DPPC exhibited a relative area change of 0.33 ± 0.02 (Figure 3 and Table 2). The main phase transition of the F6-DPPC bilayer spans over a temperature range of nearly 15 °C and is thereby substantially broader than that for DPPC bilayers (~8 °C), as determined by the ellipsometric data (Figure 3). The main phase-transition temperature was computed from the changes in bilayer thickness and from the relative area change $\Delta A/A$ to be 25.4 ± 1.2 and 28.2 ± 1.1 °C, respectively, by using an empirical sigmoidal fitting function, in agreement with the values obtained by DSC. Interestingly, F6-DPPC exhibits a strong hysteresis effects between cooling and heating cycle in the regime of T_M.[34] The ellipsometric measurements of both the membrane thickness and the relative area of the F6-DPPC bilayer did not completely recover their initial values after a heating/cooling cycle (not shown).

Discussion

We have studied the structural elements of multilamellar bilayers of the fluorinated DPPC analogue (F6-DPPC) in terms of hydrocarbon and fluorocarbon chain tilt angles by using polarized ATR-FTIR spectroscopy and examined further the relative area change and the membrane thickness during the main phase transition of single solid-supported bilayers of the respective lipids by means of temperature controlled ellipsometry and AFM.

A major structural difference between DPPC and its fluorinated analogues with respect to the bilayer structure is the strongly increased chain tilt angle θ relative to the bilayer normal. Polarized ATR-FTIR data indicate a chain tilt angle of 39° in F6-DPPC bilayers, which is 18° higher than that found for DPPC bilayers (21°). The chain tilt angle of 21° for dry multilamellar DPPC bilayers agrees with previously published data provided by Katsaras et al.,[32,44] who reported a tilt angle of the DPPC chain segment of 22° at 0% relative humidity by using X-ray diffraction.

This increase of the tilt angle was accompanied by a reduction of bilayer thickness. Both imaging ellipsometry and AFM on single bilayers indicate a step height approximately 1 nm lower in F6-DPPC than in DPPC bilayers. By using as a rough approximation very simple geometric considerations as depicted in Figure 5, this decreased bilayer thickness of F6-DPPC can be fully accounted for by the increased chain tilt angle (Table 1).

What is the physical reason for this altered lipid arrangement in the fluorinated DPPC bilayer as compared with DPPC? A likely explanation of this is depicted in the cartoon shown in Figure

6. It is well-known that the β (*sn*-2) and the γ (*sn*-1) hydrocarbon chains of diacyl phosphatidylcholines adopt a staggered conformation, resulting in a mutual offset of the terminal methyl groups of 0.25 nm.[45] In the fluorinated DPPC analogues, such a staggered arrangement of β- and γ-chains would result in partial overlap of the terminal fluorocarbon moieties and the adjacent hydrocarbon segments of the chains and would thus lead to the presence of a mixed fluorocarbon/hydrocarbon layer Δ in the lipid bilayer. Because of unfavorable fluorocarbon/hydrocarbon interaction, such a staggered conformation would be energetically unfavorable. We therefore propose that the chains adopt a different arrangement in the perfluoroalkylated lipids as compared to the nonfluorinated lipids to minimize these unfavorable interactions by avoiding chain staggering, which is commonly referred to as microphase separation. We assume that such a rearrangement of the chains can be achieved by specific rotamer populations in the glycerol moiety of the fluorinated lipids. In general, rotation about the glycerol backbone results in changes of chain staggering and possibly also leads to variations of the headgroup orientation.[46] Note that the increased tilt angle in the fluorinated DPPC analogues cannot be explained on the mere basis of an altered cross-sectional area of the fluorocarbon chain segments. On the basis of data provided by Tamada et al.,[14] the cross sectional area of the fluorocarbon chain segment is increased to 30 $Å^2$ compared to 20 $Å^2$ for the cross-sectional area of a hydrocarbon chain segment. An increase of the cross-sectional area of the chains relative to that of the headgroups should, however, lead to a decrease of the tilt angle, in contradiction with the experimental findings.

An astonishing property of the fluorinated lipids is the large upshift of the CH_2 stretching vibration during chain melting. The observed shift of 4.7 cm^{-1} during the phase transition of F6-DPPC is relatively large as compared with unfluorinated PCs, which are reported to be less than 3.0 cm^{-1} for egg PC[47] and DPPC,[48,49] covering a similar temperature difference. Because the fluorocarbon moiety of the chain has a larger cross-sectional area than the adjacent hydrocarbon moiety, the free volume for the hydrocarbon segments of the chains can be assumed to be substantially larger than in unfluorinated bilayers. This increased free volume in the fluorinated bilayers increases the probability of *gauche* conformations in the hydrocarbon segments relative to bilayers of lipids with pure hydrocarbon chains, which is directly related to the increased band shift of CH_2 stretching vibrations during the transition from the gel to the fluid phase. Molecular dynamic simulations of DPPC further revealed that the probability of *gauche* conformations is enhanced near the glycerol backbone.[50] This may further add to an increased relative population of *gauche* defects in F6-DPPC (where the five distal methylene groups per chain are replaced by CF_2 groups) as compared with DPPC. In the CF_2 chain, however, *gauche* conformations are inhibited because of steric clash of the larger fluorine substituents.[51] Notably, already in the gel phase, the CH_2 stretching vibration of F6-DPPC is at a relatively high position at 2852.5 cm^{-1} compared with that of DPPC at 2850 cm^{-1}. The reason for this higher position is not clear. It might result from special properties of F6-DPPC, such as the reduced length of the hydrocarbon segment or the presence of the neighboring fluorocarbon segment. Alternatively, it might indicate some disordering in the CH_2 segment already in the gel phase by the same mechanism of an increased free volume as detailed above. In that case, the further 4.7 cm^{-1} upshift during the transition to the fluid phase would be even more remarkable.

The unusual thermotropic properties of the fluorinated PCs can be understood as well in terms of an increased free volume of the hydrocarbon segments due to the increased cross-sectional area of the adjacent fluorocarbon segments as compared to the hydrocarbon analogue. The relative area change $\Delta A/A$ of lipid bilayers during the main phase transition is mainly caused by the occurrence of *gtg* kinks and *gauche* defects. In the fluid phase, DPPC chains are expected to have 3.9 *gauche* defects per chain at 50 °C,[52] resulting in a relative area change of more than 30% during T_M. In the F6-DPPC bilayers, the perfluoroalkylated chain segments appear to provide enough free volume for *gauche* populations in the adjacent hydrocarbon segments

to diminish the relative area change substantially, such that a $\Delta A/A$ of only 5% is observed for F6-DPPC during the transition to the fluid phase. The same effect, a larger free volume accessible to the hydrocarbon segment in the fluorinated bilayer, should also interfere with the usually occurring tight packing of the chains in the gel phase and decrease the enthalpy penalty for *gauche* conformations, thereby contributing to the considerable lowering of both the temperature and the enthalpy of the phase transition of F6-DPPC as compared to DPPC.

Conclusions

Lipids with terminally perfluoroalkylated chains have interesting bilayer properties, such as formation of highly stable vesicles[1,2] and a very distinctive domain formation in mixtures,[17,53] which make them promising candidates for a range of biomedical applications[1,9,17,54] and possible tools for clustering of ligand on liposome surfaces.[18–21] By using polarized ATR-FTIR, imaging ellipsometry, and AFM in fluids, we have investigated structural and physical properties of bilayers of a fluorinated DPPC analogue. The considerably increased tilt angle of the chains and the resulting reduced thickness of the fluorinated bilayers is presumably related to the minimization of unfavorable fluorocarbon/hydrocarbon interaction, leading to microphase separation. The decreased phase-transition temperature, on the one hand, and the drastically reduced thermal expansion and thickness change during the main phase transition of the fluorinated bilayers, on the other hand, can be understood in terms of an increased free volume accessible to the hydrocarbon chain segments due to the larger cross-sectional area of the adjacent fluorocarbon segments.

Supplementary Material

Refer to Web version on PubMed Central for supplementary material.

Acknowledgements

The authors acknowledge financial support by the NIH and NSF (to K.K.) and by Deutsche Forschungsgemeinschaft (Grant JA 963/1–4 to A.J. and Vo 811/3,4 to R.V.). R.V. thanks Fritz Siebert for discussion.

References and Notes

1. Santaella C, Vierling P, Riess JG. Angew Chem, Int Ed 1991;30:567–568.
2. Santaella C, Vierling P, Riess JG. New J Chem 1991;15:685–692.
3. Santaella C, Vierling P, Riess JG, Gulik-Krzywicki T, Gulik A, Monasse B. Biochim Biophys Acta 1994;1190:25–39. [PubMed: 8110818]
4. Frezard F, Santaella C, Vierling P, Riess JG. Biochim Biophys Acta 1994;1192:61–70. [PubMed: 8204651]
5. Frezard F, Santaella C, Montisci MJ, Vierling P, Riess JG. Biochim Biophys Acta 1994;1194:61–68. [PubMed: 8075142]
6. Santaella C, Vierling P. Chem Phys Lip 1995;77:173–177.
7. Gadras C, Santaella C, Vierling P. J Controlled Release 1999;57:29–34.
8. Rolland JP, Santaella C, Vierling P. Chem Phys Lip 1996;79:71–77.
9. McIntosh TJ, Simon SA, Vierling P, Santaella C, Ravily V. Biophys J 1996;71:1853–1868. [PubMed: 8889161]
10. Allara DL, Swalen JD. J Phys Chem 1982;86:2700–2704.
11. Chau LK, Porter MD. Chem Phys Lett 1990;167:198–204.
12. Frey S, Heister K, Zharnikov M, Grunze M, Tamada K, Colorado R Jr, Graupe M, Shmakova OE, Lee TR. Isr J Chem 2000;40:81–97.
13. Naselli C, Swalen JD, Rabolt JF. J Chem Phys 1989;90:3855–3860.
14. Tamada K, Ishida T, Knoll W, Fukushima H, Colorado R, Graupe M, Shmakova OE, Lee TR. Langmuir 2001;17:1913–1921.

15. Tsao MW, Hoffmann CL, Rabolt JF, Johnson HE, Castner DG, Erdelen C, Ringsdorf H. Langmuir 1997;13:4317–4322.
16. Ren Y, Iimura Ki, Ogawa A, Kato T. J Phys Chem B 2001;105:4305–4312.
17. Yoder NC, Kalsani V, Schuy S, Vogel R, Janshoff A, Kumar K. J Am Chem Soc 2007;129:9037–9043. [PubMed: 17602478]
18. Rai PR, Saraph A, Ashton R, Poon V, Mogridge J, Kane RS. Angew Chem, Int Ed 2007;46:2207–2209.
19. Rai P, Padala C, Poon V, Saraph A, Basha S, Kate S, Tao K, Mogridge J, Kane RS. Nat Biotechnol 2006;24:582–586. [PubMed: 16633350]
20. Nam JM, Nair PM, Neve RM, Gray JW, Groves JT. ChemBioChem 2006;7:436–440. [PubMed: 16456901]
21. Gege C, Schneider MF, Schumacher G, Limozin L, Rothe U, Bendas G, Tanaka M, Schmidt RR. ChemPhysChem 2004;5:157.
22. Charrier A, Thibaudau F. Biophys J 2005;89:1094–1101. [PubMed: 15879467]
23. Feng ZV, Spurlin TA, Gewirth AA. Biophys J 2005;88:2154–2164. [PubMed: 15596519]
24. Keller D, Niels BL, Ian MM, Ole GM. Phys Rev Lett 2005;94:025701. [PubMed: 15698195]
25. Leonenko ZV, Finot E, Ma H, Dahms TES, Cramb DT. Biophys J 2004;86:3783–3793. [PubMed: 15189874]
26. Xie AF, Yamada R, Gewirth AA, Granick S. Phys Rev Lett 2002;89:246103. [PubMed: 12484960]
27. Harrick, NJ. Internal Reflection Spectroscopy. John Wiley & Sons; NY: 1967.
28. Tamm LK, Tatulian SAQ. Rev Biophys 1997;30:365–429.
29. Goormaghtigh E, Raussens V, Ruysschaert JM. Biochim Biophys Acta 1999;1422:105–185. [PubMed: 10393271]
30. Yi PN, MacDonald RC. Chem Phys Lip 1973;11:114–134.
31. Fahmy K, Siebert F, Grossjean MF, Tavan P. J Mol Struct 1989;214:257–288.
32. Katsaras J. J Phys Chem 1995;99:4141–4147.
33. Nagle JF, Tristram-Nagle S. Biochim Biophys Acta 2000;1469:159–195. [PubMed: 11063882]
34. Schuy S, Janshoff A. ChemPhysChem 2006;7:1207–1210. [PubMed: 16676368]
35. Schuy S, Janshoff A. J Colloid Interface Sci 2006;295:93–99. [PubMed: 16112128]
36. Janshoff A, Kunneke S. Eur Biophys J 2000;29:549–554. [PubMed: 11156297]
37. Kunneke S, Janshoff A. Angew Chem, Int Ed 2002;41:314–316.
38. Faiss S, Schuy S, Janshoff A. J Phys Chem. 2007in press
39. Gang J, Roger J, Hans A. Rev Sci Instrum 1996;67:2930–2936.
40. Kim YT, Allara DL, Collins RW, Vedam K. Thin Solid Films 1990;193-194:350–360.
41. Reiter R, Motschmann H, Orendi H, Nemetz A, Knoll W. Langmuir 1992;8:1784–1788.
42. Vedam K. Thin Solid Films 1998;313-314:1–9.
43. Ganchev DN, Hasper HE, Breukink E, DeKruijff B. Biochemistry 2006;45:6195–6202. [PubMed: 16681392]
44. Katsaras J, Yang DS, Epand RM. Biophys J 1992;63:1170–1175. [PubMed: 1420933]
45. Wiederschain, GY. The structure of biological membranes. 2nd. Yeagle, PL., editor. CRC Press; Boca Raton: 2006. p. 345
46. Hauser H, Pascher I, Sundell S. Biochemistry 1988;27:9166–9174. [PubMed: 3242620]
47. Popova AV, Hincha DK. Biophys J 2003;85:1682–1690. [PubMed: 12944283]
48. Nabet A, Boggs JM, Pezolet M. Biochemistry 1996;35:6674–6683. [PubMed: 8639617]
49. Binder H. Vib Spectrosc 1999;21:151–163.
50. Smondyrev AM, Berkowitz ML. J Chem Phys 1999;110:3981–3985.
51. Rabolt JB, Fanconi B. J Polym Sci Poly Lett Ed 1977;15:121–127.
52. Douliez JP, Leonard A, Dufourc EJ. Biophys J 1995;68:1727–1739. [PubMed: 7612816]
53. Schneider MF, Andelman D, Tanaka M. J Chem Phys 2005;122:094717–094715. [PubMed: 15836172]

54. Ravily V, Santaella C, Vierling P. Biochim Biophys Acta 1996;1285:79–90. [PubMed: 8948478]

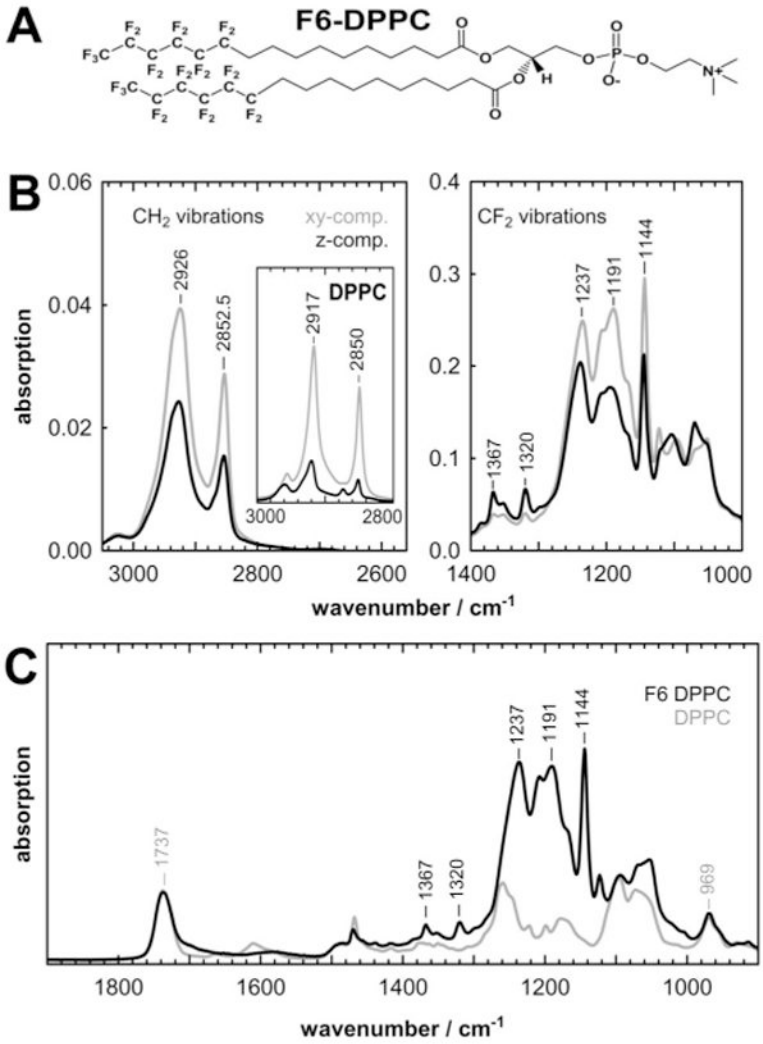

Figure 1.

ATR-FTIR spectra of dry F6-DPPC multilamellar films in the gel phase. (A) Structure of F6-DPPC. (B) Polarized ATR-FTIR absorption spectra of dry gel-phase F6-DPPC films were decomposed into the *xy*-component polarized in the plane parallel to the surface of the ATR crystal and the *z*-component polarized perpendicular to the surface. The spectra are shown in the absorption range of the CH_2 and CF_2 stretching vibrations and allow determination of the orientations of the molecular groups with respect to the crystal surface and thus the plane of the bilayer. In the inset, the corresponding polarized absorption spectra of DPPC in the CH_2 range are shown for comparison. (C) Unpolarized ATR-FTIR spectra of dry F6-DPPC films are compared with those of DPPC, revealing the bands being due to the fluorocarbon moiety (marked with black labels).

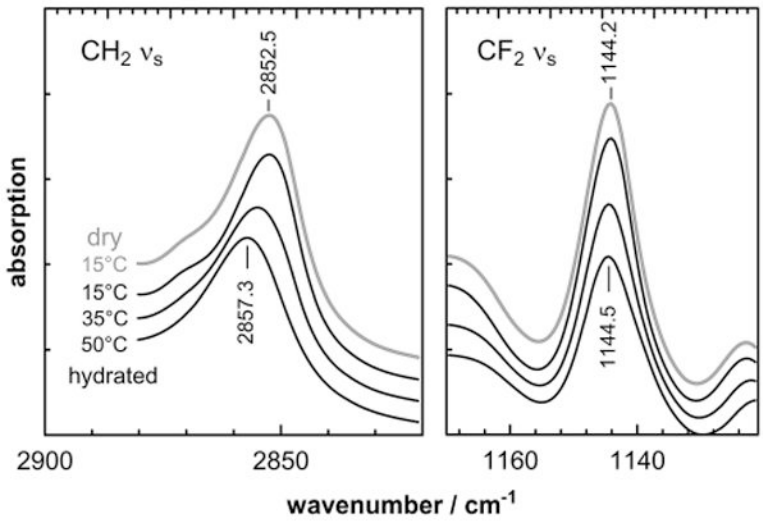

Figure 2.

ATR-FTIR spectra of the phase transition of F6-DPPC films. Spectra obtained from hydrated films at different temperatures are stacked and compared to those of a dry film at 15 °C. The symmetric CH_2 stretch (ν_S) of the hydrocarbon moiety reveals a shift from 2852.5 cm^{-1} in the gel phase to 2857.3 cm^{-1} in the fluid phase because of the increasing occurrence of *gauche* conformations in the melted phase. The symmetric CF_2 stretch vibration of the fluorocarbon moiety, on the other hand, reveals an absorption decrease and slight broadening but no significant band shift. The band positions measured in hydrated bilayers in the gel phase at 15 °C correspond to those measured in dry films at the same temperature. Tickmarks are 20 and 100 mOD in the left and right panels, respectively.

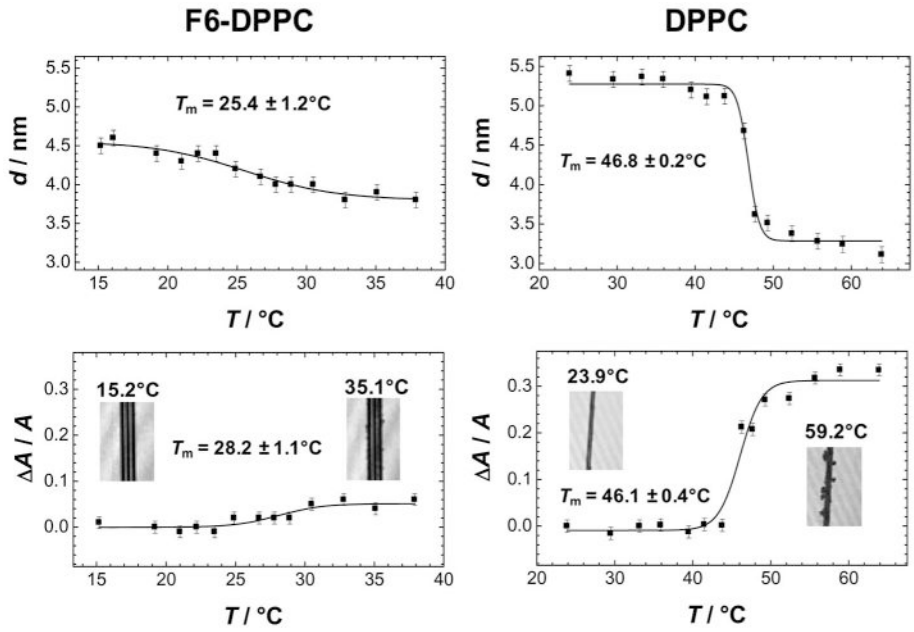

Figure 3.

Decrease of bilayer thickness *h* and relative area change Δ*A*/*A* of microstructured F6-DPPC compartments during the phase transition measured by imaging ellipsometry. A sigmoidal fit to the ellipsometric data provides temperature and width of the phase transition during a heating cycle of hydrated DPPC and F6-DPPC bilayers. Both *h* and Δ*A*/*A* data reveal a broadening of the phase transition of F6-DPPC as compared with DPPC. F6-DPPC displays a significantly lower change in thickness (0.6 nm in F6-DPPC) as compared to neat DPPC (1.9 nm in DPPC) and lower thermal expansion (5% for F6-DPPC and 33% for DPPC bilayers) by crossing the phase transition. The insets show the respective Δ-maps obtained from imaging ellipsometry of microstructured bilayers in the gel and in the fluid phase.

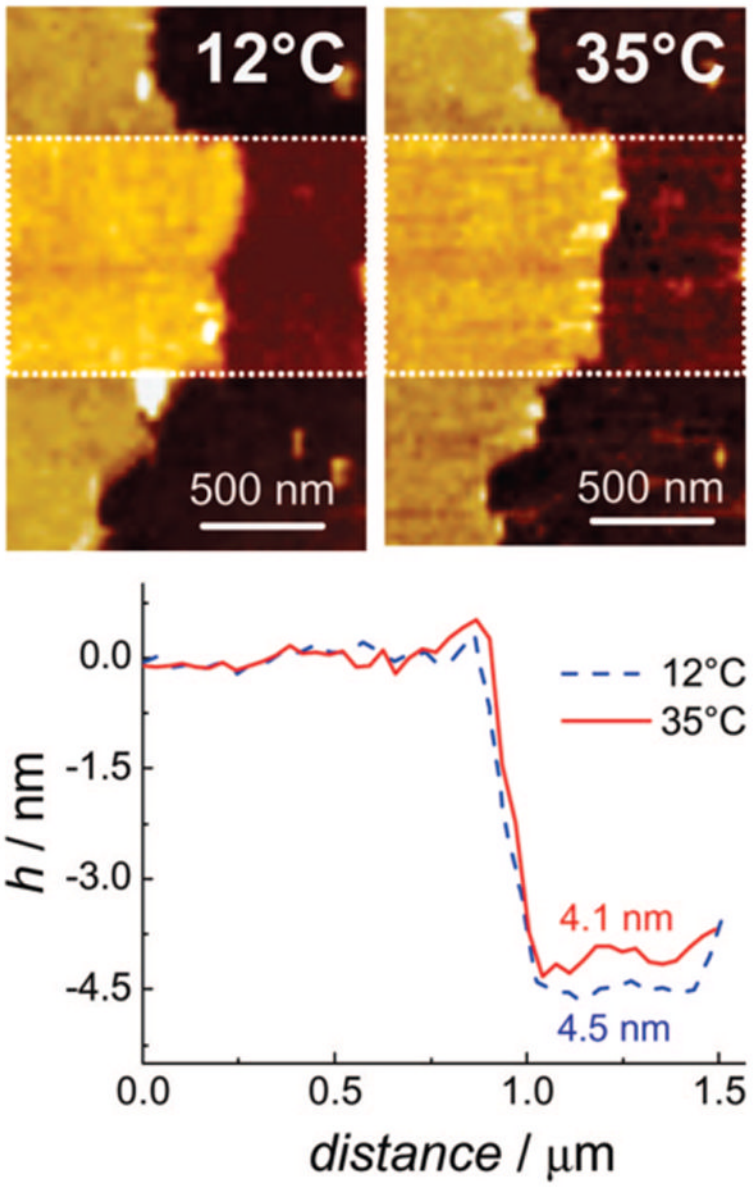

Figure 4.

Determination of bilayer thickness by AFM. AFM images of microstructured bilayers of F6-DPPC on glass were recorded in the gel phase and in the fluid crystalline phase. Averaged line scans were taken from the highlighted areas in the center of the images. The estimated error of the step height measurements is ±0.2 nm.

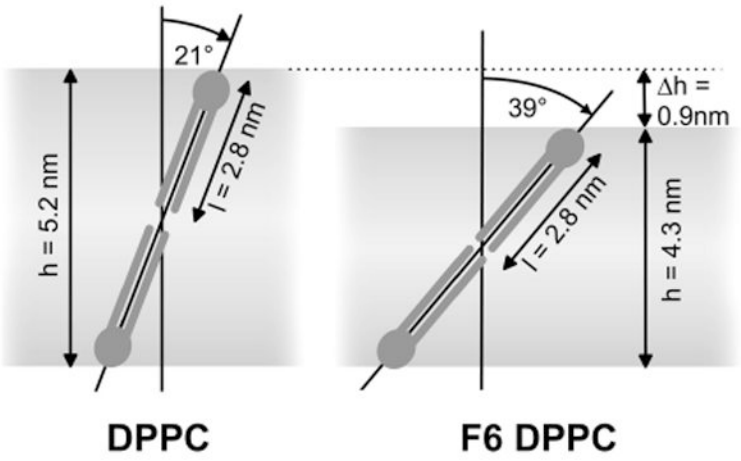

Figure 5.
Simplified geometric model to relate the bilayer thickness *h* of DPPC and F6-DPPC with the apparent tilt angle Θ. By assuming the same empirical linear length *l* of 2.8 nm for both the DPPC and F6-DPPC lipid molecules, the bilayer thickness *h* is calculated in this simplified model as 2*l* cos Θ.

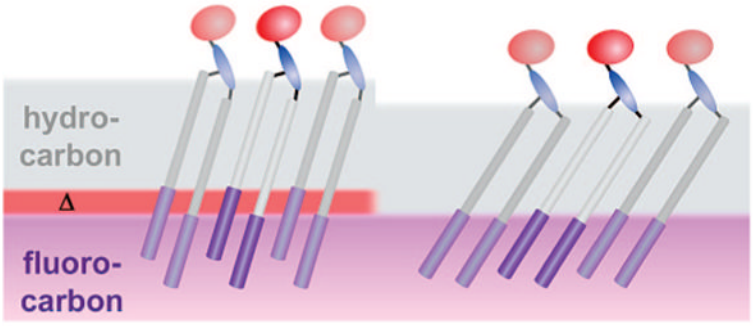

Figure 6.

A staggered chain conformation of F6-DPPC would involve unfavorable interactions because of mismatch between hydrocarbon and fluorocarbon moieties of the chains and hence the presence of a mixed hydrocarbon/fluorocarbon layer Δ, as shown schematically in the left panel of this cartoon. Such a mismatch would be minimized by a change of the chain arrangement as shown in the right panel. The minimization of these unfavorable hydrocarbon/fluorocarbon interactions is therefore suggested to be the driving force for the increased chain tilting in fluorinated DPPC.

TABLE 1

Experimental Values of the Average Tilt Angle Θ and Bilayer Thickness *h* for Lipid Bilayers in the Gel Phase

lipid	Θ,[a] deg (gel, dry film)	*h*, nm (ellipsometry)	*h*, nm (AFM)	*h*, nm (calculated)[b]
DPPC	21	5.4	5.4	5.2
F6-DPPC	39	4.5	4.5	4.3

[a] Measured by ATR-FTIR; estimated error is ±2°.

[b] Calculated from the tilt angle and the model shown in Figure 5.

TABLE 2

Experimental Values of the Bilayer Thickness *h* for Hydrated Lipid Bilayers in the Fluid Phase Determined at Sample Temperature *T* and Relative Area Change Δ*A*/*A* during the Phase Transition from the Gel to Fluid Crystalline Phase

lipid	*T*, °C	*h*, nm (ellipsometry)	*h*, nm (AFM)	Δ*A*/*A* (ellipsometry)
DPPC	60	3.4		0.35
F6-DPPC	35	3.9	4.1	0.05